MODELING OF THE SEISMIC RESPONSE OF CONCENTRICALLY BRACED STEEL FRAMES USING THE OPENSEES ANALYSIS ENVIRONMENT

[1]Antonio Agüero, [2]Carmen Izvernari and Robert Tremblay

[1]Departamento de mecánica de los medios continuos y teoría de estructuras
ETS de ingenieros de Caminos, Canales y Puertos, Universidad Politécnica de Valencia
Campus Vera s/n, 46020 Valencia, España, Email: anagra@mes.upv.es

[2]Department of Civil, Geological and Mining Engineering
Ecole Polytechnique of Montreal, Montreal (QC) Canada H3C 3A7

ABSTRACT: A study was performed to investigate the possibility of modeling the seismic inelastic cyclic response of steel bracing members using the OpenSees computer program. The study focuses on bracing members made of rectangular and square steel tubes. The efficiency and the accuracy obtained from the force (FBE) and displacement (DBE) based elements are first compared. A co-rotational framework is used to model the nonlinear geometric behavior, and inelasticity is accounted for through fiber discretization of the cross-section together with bi-linear or Giuffré-Menegotto-Pinto hysteretic material response. FBE and DBE models are compared for various combinations of number of elements along the brace length, number of integration points along the element length, number of fibers used to define the cross-section, and amplitude and number of displacement increments. The influence of brace slenderness and displacement protocol on the accuracy of the models is examined. Model predictions are also compared to individual brace and full-scale frame test results. The influence of time step and brace discretization on the dynamic seismic response for a typical braced steel frame is investigated.

Keywords: Displacement based element; Force based element; Braces; Buckling; Yielding; Gusset plate; Frame; Earthquakes; Seismic.

INTRODUCTION

Three types of derivation have been mainly used to study the nonlinear dynamic behavior of three-dimensional structural systems that include beam elements with hysteretic behavior under a predominantly uniaxial state of strain and stress: displacement, flexibility and mixed formulations. Bracing members in braced steel frames are expected to experience several cycles of inelastic buckling and tensile yielding when the structure is subject to strong seismic ground motions (Fig 1). When modeling the behavior of braced frames under seismic loading, the type of brace model and related numerical aspects must therefore be carefully selected such that accurate results can be obtained while minimizing the computation costs.

The Open System for Earthquake Engineering Simulation (OpenSees) (McKenna and Fenves, 2004) is a software framework using finite element methods to develop applications for the simulation of the performance of structural and geotechnical systems subjected to earthquakes. OpenSees is comprised of a set of modules to perform creation of the finite element model, specification of an analysis procedure, selection of quantities to be monitored during the analysis, and the output of results. A large-displacement buckling formulation with a fiber representation of sections incorporated in OpenSees has already been used to reproduce the inelastic cyclic response of steel bracing members (Uriz and Mahin, 2004). The objective of this study is to develop guidelines for modeling the non-linear seismic response of steel braces using this type of formulation. The displacement and force based formulations are compared with consideration of the number of elements, integration points, and fibers on the evaluation of brace response parameters.

The accuracy of the FBE model for different brace slenderness and applied loading protocols is examined. FBE model predictions are then compared to the results of tests performed on 4 individual brace tests. Full-scale tests results are then used to evaluate the brace modeling technique with rotational springs simulating end restraint conditions imposed by the gusset connections. Finally, the accuracy of the proposed brace model is investigated for the dynamic seismic analysis of a single-storey X-braced steel frame.

FORCE BASED ELEMENTS VS DISPLACEMENT BASED ELEMENTS.

In the force based element (mixed formulation), compatibility and equilibrium equations are satisfied in a weak sense. The implementation is based on the Hellinger-Reissner (H-R) variational principle with the weak form of the equilibrium equations: $\iiint \sigma \cdot \delta\varepsilon^T \cdot dV - \delta d^T \cdot F_{EXT} = 0$. The strains $\{\varepsilon\}$ are derived from the displacements $\{d\}$ using $\varepsilon_1 = L \cdot d$, where $\{L\}$ is the differentiating operator, and from the stresses $\{\sigma\}$ using $\sigma = C \cdot \varepsilon_2 \rightarrow \varepsilon_2 = C^{-1} \cdot \sigma$, where C is the material constitutive laws. The weak form of the compatibility equation $\iiint W \cdot (\varepsilon_1 - \varepsilon_2) dV = 0$ is used, where $\{W\}$ is a weight residual function and, hence, the H-R principle leads to: $\iiint \sigma \cdot \delta\varepsilon^T \cdot dV - \delta d^T \cdot F_{EXT} + \iiint W \cdot (\varepsilon_1 - \varepsilon_2) dV = 0$. In the displacement based formulation, equilibrium equations are satisfied in a weak sense, with a displacement field assumed in each element. The strains are derived from the displacements using $\varepsilon_1 = L \cdot d$, and the stresses from the strains with $\sigma = C \cdot \varepsilon_1$. The weak form of the equilibrium equation takes the form: $\iiint \sigma \cdot \delta\varepsilon^T \cdot dV - \delta d^T \cdot F_{EXT} = 0$.

A first parametric study was performed to compare the efficiency of both element formulations. A co-rotational framework was used to model the nonlinear geometric behavior, and spread of inelasticity was accounted for through fiber discretization of the cross-section with bi-linear hysteretic material behavior with isotropic and kinematic strain hardening. In the analyses, an initial sinusoidal out-of-straightness with maximum amplitude of $1/500^{th}$ of the brace length was considered, as prescribed in standards for the fabrication of structural tubing (e.g., ASTM, 2003). The tolerance was set to 10^{-7} and a displacement step size of 0.1 mm was used. The analyses were performed for the brace specimen S2A tested by Tremblay et al. (2003). This brace had a rectangular tubular cross-section (HSS 102x76x4.8) with a steel Young's modulus, E, of 185 GPa and steel yield stress, F_y, of 381 MPa. The slenderness parameter of the brace, $= (P_y/P_{cr})^{0.5}$, was equal to 1.56, where P_y and P_{cr} are the squash load and the elastic buckling load of the brace, respectively. The number of elements along the brace length, n_e, was varied (n_e = 4, 8, 16, 24, and 32), as well as the number of integration points per element, n_i (n_i = 4, 5, and 6). A total of 16 fibers were used for modeling the cross-section, as illustrated in Fig. 2a. Typical hysteresis responses obtained from computation are shown in Fig. 2b.

The computational work was performed with a Pentium 4 with 2.8 GHz and 1.0 Gb RAM. The computation time is given in Fig. 3a as a function of the number of elements and integration points. As shown, the computational effort increases nearly linearly with the number of elements but is not influenced by the number of integration points. For this particular example, it was found that the force based formulation required between 40% and 50% more calculation time than the time needed with the displacement based formulation. In the parametric study, it was observed that the sequence of analyses had an influence on the computational time when using the Tcl programming language. This was not the case when the Python programming language was used to control a

series of OpenSees analyses.

The mean quadratic error on the force developed by the brace element, *MQE,* was determined using $MQE = [\quad (P_i\text{-}P_{ie})^2/n]^{0.5}$, where P_i are the force estimates at every calculation step with a given (n_e, n_i) combination and P_{ie} are the force values determined with $n_e = 32$ and $n_i = 6$, and n is the number of calculation steps. The error *MQE* is expressed as a percentage of the brace yield load, P_y. Figure 3b shows the variation of *MQE* with the parameters n_e and n_i. The numerical results are presented in Table 1. As anticipated, the error decreases with the number of elements. Again, the number of integration points had a limited impact on the quality of the results. The figure clearly shows that a force based formulation leads to more accurate results. Such a convergence is in agreement with previous studies (e.g., Barbato and Conte, 2004).

PARAMETRIC STUDY USING THE FORCE BASED FORMULATION

Influence of modeling parameters

A second parametric study was carried out using the forced based formulation. The influence of brace slenderness was examined by carrying out analyses on three braces with different cross-sections and effective lengths. The properties of the braces are given in Table 2. All members were tubular steel shapes with square cross-sections made of ASTM A500 grade C steel with F_y = 345 MPa and E = 200 GPa.

The initial out-of-straightness conditions considered in the previous study were also specified in this second series of analyses. However, the uniaxial Giuffré-Menegotto-Pinto (GMP) steel material with kinematic and isotropic hardening was used to simulate Bauschinger effect under cyclic loading. The properties specified for this model were based on the load-deformation response measured on the core of buckling restrained bracing members subjected to quasi-static cyclic testing (Tremblay et al., 2004). In the GMP model, the transition between elastic to plastic response was characterized by the following parameters: $R_0 = 25$, $cR_1 = 0.925$, $cR_2 = 0.15$, the isotropic hardening parameters were: $a_1 = a_3 = 0.00001$, $a_2 = a_4 = 0.00002$; and the kinematic hardening parameter, b, was set equal to 0.01.

In Fig. 4, the experimental measurements are compared to the analytical predictions from the bi-linear model used in the previous study and the GMP model. As shown, the second model better reflects the cyclic hysteretic behavior of steel material. Figure 5 compares the response obtained using the bilinear and the GMP hysteretic brace model. When compared to typical measured response (see Fig. 1), the later provides a more realistic representation of actual brace behavior with smoother transitions between elastic and inelastic stages.

The test loading protocol proposed for buckling restrained braces (AISC, 2005) was applied in the study: 6 cycles at a brace axial deformation, δ, equal to δ_y, 4 cycles at $\delta = 0.5\ \delta_m$, 4 cycles at $\delta = 1.0\ \delta_m$, and 2 cycles at $\delta = 2.0\ \delta_m$, where δ_y is the axial deformation at yield and δ_m is the brace deformation at design storey drift, $\delta_m = 3.2\ \delta_y$. The modeling parameters that were varied included the number of elements along the brace length (n_e = 4, 8, 16 and 32) and the number of fibers used to define the cross-section, n_f = 8, 12 and 16. Prior to performing the study, preliminary analyses were carried out on the intermediate slenderness brace ($\lambda = 1.0$) with n_i = 3 and 4 (number of integration points per element). No significant differences could be observed for the *MQE* and the total energy dissipated by the brace that were computed with these two n_i values. Therefore the number of integration points was set equal to 3.

A total of 8 response parameters describing the brace hysteresis response were examined: 1) the buckling load at first occurrence of buckling, P_{u0}; 2) the buckling load in the first cycle at $\delta = 1.0\ \delta_m$, P_{u1}; 3) the energy dissipated up to and including the 4th cycle at $\delta = 1.0\ \delta_m$, E_{h1}; 4) the energy dissipated at the end of the test loading protocol, E_{h2}; 5) the brace deformation when developing P_y in the first cycle at $\delta = 1.0\ \delta_m$, δ_{y1}; 6) the compressive resistance at peak negative deformation in the first cycle at $\delta = 1.0\ \delta_m$, P_1; 7) the brace out-of-plane deformation at peak negative deformation in the first cycle at $\delta = 1.0\ \delta_m$, Δ_1; and 8) the brace out-of- plane deformation at peak negative deformation in the first cycle at $\delta = 2.0\ \delta_m$, Δ_2.

The variation of the 8 brace response parameters as a function of n_e and n_f is presented for each brace slenderness in Fig. 6. For each brace slenderness, the results have been divided by the values obtained with the highest level of discretization, i.e. using $n_e = 32$ and $n_f = 16$. Clear trends can be observed from these plots: the quality of the results is maintained when the number of elements is reduced from 32 to 8, but it degrades significantly if the number of fibers is reduced from 16 to 8. For $n_f = 16$, discretizing the brace members with 8 elements instead of 32 elements resulted in errors of only 1% or less for all parameters except for P_{u1} for $\lambda = 1.0$ in which case the error reached 3%. The same trend is observed for other values of n_f. Conversely, the loss in accuracy can reach up to 10% (δ_{y1} for $\lambda = 1.0$) or 5% (other response parameters or slenderness) when n_f is reduced from 16 to 12 and n_e is kept equal to 32. Much larger errors are observed if n_f is reduced further from 12 to 8. It is noted, however, that the stockiest brace is less sensitive to a reduction in the number of fibers (error less than 3% when n_f is reduced from 16 to 12 and n_e is reduced from 32 to 8).

Influence of loading sequence

The analyses on the three bracing members were redone under two additional loading sequences: the quasi-static cyclic test protocol recommended by the European Convention for Constructional SteelWork (ECCS, 1991) and the brace test displacement history that was developed by Tremblay and Bouatay (2002) for braced steel frames exposed to crustal and sub-crustal earthquakes in western Canada (WC protocol). The response under the AISC loading protocol is also considered for comparison. The three displacement sequences are illustrated in Fig. 7. The history of the energy dissipated, E_H, as a function of the cumulated imposed displacement, $\Sigma\delta$, in each loading protocol is used to evaluate the validity of the modeling assumptions. The stockier ($\lambda = 0.5$) and the most slender ($\lambda = 2.0$) braces are examined. Two different models are considered: a simple but still accurate model as per previous studies with $n_e = 8$, $n_f = 16$, and $n_i = 3$, and a more refined model with $n_e = 32$, $n_f = 16$, and $n_i = 4$. As shown in Fig. 7, the simple model predicts equally well the brace energy dissipation capacity, regardless of the model assumptions and the applied loading history. The total energy dissipation capacity is compared in Table 3. Again, negligible differences are found between the two models.

VALIDATION AGAINST BRACE TEST RESULTS

The force based formulation is used to reproduce the hysteretic response of four rectangular HSS bracing members from different test programs. The properties of the braces are given in Table 4. Specimens S2-A and S1QB were tested by Tremblay et al. (2003) while tests on Specimens 1B and 2 were respectively performed by Shaback and Brown (2003) and by Haddad (2004). The cross-sectional flexural properties, I and r, are those associated with the plane of buckling observed in the tests. The $_y$ values are reference yield deformations as defined in each of the studies. Initial out-of-plane imperfections at mid-length of the braces, v_0, as assumed in the analyses, are also

given in the table.

According to current seismic design practice, brace connections must be detailed to allow ductile rotational response upon brace buckling. For single gusset plate connections, end rotations due to out-of-plane brace buckling can be easily accommodated in the gusset plates by introducing a free hinge length between the brace end and the line of restraint (see Fig. 8a). It is recommended that the length of the free hinge region be equal to two times the gusset plate thickness, t_g (Astaneh et al., 1985). This detail was adopted in the three test programs, as shown in Fig. 8b for the tests by Tremblay et al. (2003), and the length L in Table 4 corresponds to the brace length between hinge center lines.

Such a detail induces rotational restraint at the brace ends, and plastic hinging is anticipated in the gusset plates when large brace out-of-plane deformations develop after brace buckling in compression (see Figs. 8b and 8c). Using the flexural stiffness of the gusset plate assembly, C_g, the brace effective length including end restraint effects can be determined from classical elastic stability theory (Chajes, 1974). Table 5 gives the values of C_g for each of the test specimens as well as the resulting slenderness parameters. For these braces, the parameter K varies from 0.75 to 0.93. In view of the key role of the brace effective slenderness on the cyclic hysteretic response of bracing members, these end condition effects must be properly modeled when reproducing brace test results or predicting the brace response in actual building structures. Three different approaches are presented in the following sub-sections to account for the rotational restraint induced by the gusset plates.

Brace model with effective length KL

In the first modeling approach, a pin-ended brace is used with a length equal to the brace effective length KL (see Fig. 8d). In Fig. 9, the predicted response with n_f = 16, n_i = 3, and n_e = 8 is compared to the test measurements for Specimens S2A and 2. Similar results were obtained for the other two test braces or when using a larger number of elements (n_e greater than 8). Hysteretic responses are compared using two set of parameters for the Giuffré-Menegotto-Pinto material model. The curves on the left hand side were obtained with the same parameters as defined in the previous section, i.e. with R_0 = 25 and both isotropic and kinematic strain hardening properties. In the second comparison, the parameter R_0 was reduced to 20 and isotropic hardening was omitted (a_1 to a_4 = 0.0). It can be seen that using a lower R_0 value with more progressive yielding behavior resulted in a better match with the measured response for the post-buckling resistance upon reloading in compression at large deformations. When isotropic hardening was specified, the predicted yield tensile resistance of the braces was found to increase with the number of cycles, which was not the case for the test specimens. As shown, a material model without isotropic hardening seems to be more appropriate. This modified GMP material model is used in the remaining of the paper.

Although the GMP steel model closely reproduces the transition between tension and compression responses, it must be realized that it has inherent limitations such that it will not be possible to exactly characterize brace cyclic inelastic response. For instance, residual stresses are not included in the model. This leads to a generally stiffer response in the first loading cycles with small deformations, as well as a higher compression load at first occurrence of buckling. Local buckling and brace fracture cannot be reproduced either. Therefore, the predicted response would generally be too optimistic near the end of a test, when degradation in strength and stiffness is typically observed due to local buckling and progressive cracking of the cross-section.

The pin-ended brace model of length KL also has drawbacks that may preclude its use in seismic

building analysis. One of these limits is the fact that the length of the brace model does not correspond to the actual brace length in the structure. In the individual brace analyses carried out herein, the test loading protocol was multiplied by K before it was applied to the numerical model. Therefore, the same elastic and inelastic deformation demand could be imposed in both the test and model braces. This cannot be done in a building analysis. The gaps can be filled with additional beam-column elements with same cross-sectional area and infinite flexural stiffness and strength, but the amount of inelastic deformations imposed on the brace portion of length KL would be overestimated. A second main shortcoming of the KL model is the fact the model will always underestimate the out-of-plane brace deformations due to the shorter brace length, as illustrated for Braces S2A and 2 in Fig. 9c. This affects the brace post-buckling compression capacity as well as its resistance upon straightening the brace in tension. Finally, a model based on the effective length cannot capture the energy dissipation that develop at the braces ends through plastic hinge rotations in the gusset plates.

Brace model with end extensions

The problems of the KL model associated with the difference between actual and model brace lengths can be partly overcome by using the model shown in Fig. 8e. In this model, the rotational restraints at the brace ends are included by adding fictitious brace extensions of length L_c at both ends of a brace model having the actual brace length. The out-of-plane displacements at the outer ends of these extensions must be restrained. For simplicity, the flexural stiffness (EI) of the bracing member can be assigned to the extensions. If pinned connections are specified at the outer ends of the extensions, the length L_c can then be taken equal to $3EI/C_g$. The L_c values so computed for the four brace specimens are given in Table 5, and Figure 10 compares the response of Specimen S2A obtained from this model to the test results and the predictions from the KL model. All calculations were carried out with $n_f = 16$, $n_i = 3$, and $n_e = 8$.

As shown, both the KL model and the model with extensions give virtually the same response for this specimen. The use of brace extensions however permits to reproduce adequately the out-of-plane deformations (Fig. 10c). It must also be noted that the energy dissipation in the gusset plates can be included in this model by specifying the plastic moment resistance of the gusset plates for the extension members. In the analysis of actual braced frame structures, however, the modeling of the extensions and the support conditions at the outer ends of the brace extensions can still represent a challenge for the analyst and a more convenient model should be developed for that purpose.

Brace model with rotational springs

In the third option, the flexural restraint at brace ends is incorporated by means of zero-length rotational springs. The simplest models would include linear elastic springs with a stiffness C_g. More sophisticated representation can however be considered to reproduce the hysteretic response of the gusset plates under the successive bending cycles imposed at every brace load reversal. Such a refined modeling is adopted herein in which the rotational springs were given the flexural stiffness and strength of the gusset plates (C_g and M_{pg} in Table 5). In addition, the GMP steel model that was used for the braces was also applied for the gussets.

In this model, the brace length corresponds to the actual brace length and flexural strength is assigned to the gusset plates. In frame analysis, torsional restraint of the brace and gusset plates can also be included when out-of-plane buckling is studied. Brace torsional properties must then be added to the fiber nonlinear beam-column element using the aggregation tool in OpenSees. One limitation of the model is that the flexural strength of the rotational spring does not vary as a

function of the axial load applied by the brace to the gusset plate. Therefore, the spring resistance in the gusset model can be overestimated when high axial loads are transmitted by the gusset, as is the case when tension yielding develops in the braces. Figure 11a shows the predicted M-θ hysteretic response of the upper gusset plate of Specimen S2A. The predicted and measured brace end rotations are also compared for this specimen. Again, n_f = 16, n_i = 3, and n_e = 8 were used in these calculations. Due to its limitations, the model tends to overestimate the end rotations at large brace deformations, as a result of the permanent rotation that gradually develops upon load reversals due to the too high flexural resistance. However, the very good match between test and predicted axial and out-of-plane brace responses in Figs. 11c and 11d suggest that this error has limited impact on brace overall behavior.

Figure 12 compares the predicted hysteretic and out-of-plane responses of the three remaining brace specimens. Again, excellent match is obtained in all cases except for the axial load prediction during the large positive deformation excursion tension for Specimen SQ1B. This difference can be attributed to the methodology used to measure F_y in the tests (2% offset method), as this approach does not capture well progressive yielding including residual stress effects observed in HSS members. The figure also shows that the model can overestimate the peak compression brace resistance at first buckling, likely because residual stresses are not included in the model. Again, degradation of brace tension capacity due to local buckling and material fracture is not captured by the model. Table 6 compares the test and predicted total energy dissipated by the brace up to the point of zero deformation in the last tension half-cycle before fracture. As shown, the models generally underestimate the energy dissipated by the braces, especially for Specimen S1QB due to the error in predicting the measured yield tensile resistance. The results however show that little error is induced when using 8 elements to discretize the braces.

INELASTIC FRAME ANALYSIS

Comparison with test results

The overall response of the test X-braced frame by Tremblay et al. (2003) with Specimen X6-C is compared to that of the model analysis. The frame is shown in Fig. 13a. In the test, true pinned connections were built at the column bases and at the beam-to-column joints such that the applied lateral load was entirely resisted by the braces. The braces were HSS 64x64x4.8 with the following properties: A = 1060 mm^2, r = 23.6 mm, F_y = 397 MPa, E = 189 GPa, KL/r = 89.8, λ = 1.31, and J = 995x10^3 mm^4. At brace intersection, one brace was continuous whereas the other brace was interrupted. However, as shown in the figure, full torsional and flexural continuity was restored between the two brace segments by means of welding and connecting plates. The braces were connected at their ends with gusset plates 300 mm wide by 9.5 mm thick. At the lower brace ends, the gusset plates were connected to the frame columns. At the top ends, the gussets were welded to the beam only. Beam and column properties are given in Fig. 13b. For this frame, the yield storey shear, V_y, is defined as the sum of the horizontal components of the brace tension yield capacity: V_y = 674 kN. The yield story drift, Δ_y, is equal to 12.1 mm.

A general purpose model was developed with rotational springs at beam-to-column joints (C_1), and with springs exhibiting rotational and torsional properties at brace ends (C_2 *and* C_3) and at the connection between the two braces (C_4). For this particular test application, C_1 = 0, C_2 = 29 kN-m/rad (flexure) and 45 kN-m/rad (torsion), and C_3 = 37 kN-m/rad (flexure) and 45 kN-m/rad (torsion). The flexural capacity of springs C_2 and C_3 was set equal to 2.045 kN-m. Springs C_4 was given infinite stiffness and strength in flexure and torsion. As mentioned earlier, the torsional properties of the braces had to be added to the fiber beam-column brace elements to capture their

torsional reponse. The frame was subjected to a symmetrical displacement protocol with stepwise incremental amplitudes. The braces were modeled using the GMP steel material with the properties as defined in the previous section. The parameters n_f = 16 and n_i = 4 were used, and the number of elements in each of the half-brace segment was varied as followed: n_e = 2, 4, 8, and 16. The shape of the initial brace out-of-straightness was set to match the observed buckling mode.

Figures 14a to 14c compare the measured and predicted lateral load-lateral deformation response of the frame as well as the out-of-plane deformation response at mid-length of the lower half-brace segment of the continuous brace and at the brace intersection point. The results shown were obtained using 4 elements for each of the half-brace segments. Excellent agreement is found between the experimental and computed results. Figs. 14d and 14e show the influence of the number of elements on the global hysteretic response and the energy dissipated by the frame, E_H. The cumulated energy dissipation in the test was equal to 26.1 $V_y\Delta_y$. The analysis results are 23.8, 22.7, 22.2, and 22.2 $V_y\Delta_y$ with n_e = 2, 4, 8, and 16, respectively. These results again show that a total of 8 elements per brace would be adequate to properly reproduce the behavior of braces of this type.

Seismic analysis

The response of an actual single-storey X-braced steel frame subjected to an earthquake ground motion is examined to assess the validity of the model for inelastic seismic response analysis. The building plan dimensions are 45 m x 45 m and its height is 3.658 m. The structure is located in Victoria, B.C., Canada, on a stiff soil site. The design was performed according to the provisions of the 2005 National Building Code of Canada (NRCC, 2005) and the CSA-S16-01 Standard for the design of steel structures in Canada (CSA, 2001). Steel with nominal F_y = 345 MPa, E = 200 GPa, and G = 77 GPa is used for all members. For simplicity, the roof diaphragm is assumed infinitely stiff and the total seismic weight (5508 kN) is concentrated at the roof level. A single braced bay, 9.0 m wide, is used on each of the exterior walls and tension-only design was assumed. The bracing members are HSS 102x102x6.4 with the following properties: A = 2170 mm^2, r = 38.6 mm, KL/r = 113, λ = 1.50, J = 5320x10^3 mm^4. The braced bay columns are HSS 152x152x4.8 (A = 2570 mm^2, I = 9.27x10^6 mm^4) and the beams are W460x60 (A = 7590 mm^2, I = 255x10^{6}mm^4). The base of the columns is assumed to be pinned and simple shear connections are used between the beams and the columns. The fundamental period of the structure is 0.55 s if the compression braces are neglected. It reduces to 0.38 s when the contribution of the compression braces is included.

The model in Fig. 13b can be employed for this structure. An expected yield strength F_{ye} = 385 MPa was used for the braces and gusset plates. Spring C_1 was given zero stiffness. Springs C_2 and C_3 both have a flexural stiffness of 173 kN-m/rad and a flexural strength of 5.42 kN-m for out-of-plane bending. They were considered as infinitely stiff for in-plane bending and their torsional stiffness was set equal to 216 kN-m/rad for spring C_2 and 227 kN-m/rad for spring C_3. Spring C_4 was defined as fully rigid in all three rotational axes, assuming the same type of connection as in test frame X6-C. The rigid extensions at the lower and upper brace ends are respectively 353 mm and 843 mm long.

The analysis is carried out under a record from the 1994 **M**7.0 Northridge earthquake (Station Standford University, Component 0°). The record was scaled by 1.43 to match the design spectrum and to account for accidental building eccentricity effects. The brace model was used with n_f = 16, n_i = 4, and different values for n_e: 4, 8, and 16. The tolerance was set to 10^{-3} and the Newton-Raphson with line search algorithm was adopted to improve the convergence. Time step values, Δt, of 0.01 s and 0.001 s were used. In analyses performed with time steps longer than 0.01 s, convergence could not be reached upon first brace buckling. Mass proportional Rayleigh

damping was used with 5% in the first structure mode (T_1 = 0.38 s).

Figures 15a compares the time history of the roof horizontal displacement for the two time steps and n_e = 4 and 16. The time history of the energy dissipated in the system for Δt = 0.01 s is also given in the figure. Figure 15b shows the hysteretic response obtained for n_e = 4 when using Δt = 0.01 and 0.001 s, showing the effect of brace response degradation on the lateral strength and stiffness of the frame under cyclic loading. For Δt = 0.01s, the total energy dissipated by the braces with n_e = 4, 8, and 16 is respectively equal to 6.27, 6.28 and 6.29 $V_y\Delta_y$. For Δt = 0.001 s and n_e = 4, E_H = 6.36 $V_y\Delta_y$. These results clearly indicate that good predictions can be achieved for typical braced frames similar to the one studied herein by using a time step of 0.01 s and 4 elements per half-brace segment.

CONCLUSIONS

Parametric studies were carried out to evaluate the influence of modeling assumptions when simulating the hysteretic response of steel bracing members with the OpenSees finite element computer program. Nonlinear beam-column elements were used with a fiber representation of member cross-sections. The study showed that the number of integration points per element has limited influence on the response and that accurate results could be obtained with three integration points. For a given set of parameters, the force based formulation was found to provide higher accuracy compared to the displacement based formulation. This formulation should therefore be preferred, even if it requires longer computational time. As expected, the errors were found to reduce when increasing the number of elements or the number of fibers. The results indicate that sufficient accuracy could be achieved for typical bracing members if 8 elements per brace member were used together with 16 fibers for cross-section discretization. The use of the Giuffré-Menegotto-Pinto constitutive model was also found to provide a more realistic representation of the brace hysteretic response compared to the simpler bi-linear model. Comparisons between test and predicted results as well as simple dynamic seismic analysis confirm the appropriateness of these modeling assumptions for typical low-storey braced frame applications.

The brace model was found to give realistic predictions of the hysteretic response of braces having different sizes, slenderness ratios or end restraint conditions. This is by far superior to using empirical or semi-empirical models which specific test data are needed to adequately reproduce key response properties. However, the brace modeling considered in this study still has some limitations. For instance, it does not account for residual stress effects on compression strength at first buckling, and local buckling effects and brace fracture cannot be reproduced by the model. It is recommended that future work be devoted to implement local buckling effects as well as brace fracture by means of a damage model, such as the one proposed by Jin and El-Tawil (2003).

ACKNOWLEDGEMENTS

This research was supported by the Natural Sciences and Engineering Research Council of Canada. The authors also wish to acknowledge J. Brad Shaback and Madhar Haddad for providing test data as well as Charles-Philippe Lamarche for his valuable contribution in the analysis of the frame structures.

REFERENCES

[1] AISC. 2005. *ANSI/AISC 341-05, Seismic Provisions for Structural Steel Buildings*. American Institute of Steel Construction. Chicago, Il.

[2] Astaneh-Asl, A., Goel, S.C. and Hanson, R.D. 1985. Cyclic Out-of-Plane Buckling of Double-Angle Bracing. *J. of Struct. Eng., ASCE,* 111, 1135-1153.

[3] ASTM. 2003. *ASTM A500-3, Standard Specification for Cold-Formed Welded and Seamless Carbon Steel Structural Tubing in Rounds and Shapes,* ASTM International, West Conshohocken, PA.

[4] Barbato, M. and Conte, J.P. 2004. Finite Element Response Sensitivity Analysis: a Comparison Between Force-Based and Displacement-Based Frame Element Models. *Computer Methods in Applied Mechanics and Engineering*, 194, 1479-1512.

[5] Chajes, A. 1974. *Principles of Structural Stability Theory*. Prentice-Hall, Inc., Englewood Cliffs, NJ.

[6] CSA. 2001. *CSA-S16-01, Limit States Design of Steel Structures*. Canadian Standards Association, Toronto. ON.

[7] ECCS. 1986. *ECCS – TWG 1.3 Seismic Design Recommended Testing Procedure for Assessing the Behaviour of Structural Steel Elements under Cyclic Loads.* European Convention for Constructional Steelwork, Technical Committee - Structural safety and loading, Brussels, Belgium.

[8] Jin, J. and El-Tawil, S. 2003. Inelastic Cyclic Model for Steel Braces. *J. of Eng. Mech., ASCE*, 129, 5, 548-557.

[9] Haddad. M. 2004. Ph.D. Thesis. Dept. of Civil Eng., Univ. of Calgary, Calgary, AL.

[10] McKenna, F. and Fenves, G.L. 2004. *Open System for Earthquake Engineering Simulation (OpenSees)*. Pacific Earthquake Engineering Research Center (PEER), University of California, Berkeley, CA. (http://opensees.berkeley.edu/index.html)

[11] NRCC. 2005. *National Building Code of Canada, 12th ed.*, National Research Council of Canada, Ottawa, ON.

[12] Shaback, J.B. and Brown, T. 2003. Behaviour of square hollow structural steel braces with end connections under reversed cyclic axial loading. Can. J. Civ. Eng., 30, 745–753.

[13] Tremblay, R., Poncet, L., Bolduc, P., Neville, R., and DeVall, R. 2004. Testing and Design of Buckling Restrained Braces for Canadian Application. *Proc. 13th World Conference on Earthquake Eng.*, Vancouver, BC, Paper no. 2893.

[14] Tremblay, R., Archambault, M.-A., and Filiatrault. A. 2003. Seismic Performance of Concentrically Braced Steel Frames made with Rectangular Hollow Bracing Members. *J. of Struct. Eng., ASCE,* **129:12**, 1626-1636.

[15] Tremblay, R. and Bouatay, N. 2002. Loading Protocols for the Seismic Testing of Ductile Bracing Members in Concentrically Braced Steel Frames. *Proc. 12th European Conf. on Earthquake Eng.*, London, UK, Paper No. 480.

[16] Uriz, P. and Mahin, S. A. 2004. Seismic performance Assessment of Concentrically braced steel Frames. *Proc. 13th World Conference on Earthquake Eng.*, Vancouver, BC, Paper No. 1639.

TABLE 1 Mean quadratic error values (% P_y)

n_e	Displacement based elements			Force based elements		
	$n_i = 4$	$n_i = 5$	$n_i = 6$	$n_i = 4$	$n_i = 5$	$n_i = 6$
4	20.1	20.1	20.0	12.5	12.5	12.4
8	4.80	4.95	4.86	2.22	2.12	2.10
16	1.32	1.29	1.27	0.68	0.74	0.65
24	0.61	0.61	0.61	0.19	0.15	0.14
32	0.02	0.04	0.00	0.05	0.05	0.00

TABLE 2 Brace properties

Shape	A (mm^2)	$I_x = I_y$ (10^6 mm^4)	r (mm)	KL (mm)	KL/r ( )	λ ( )
305x305x16	16100	222	118	4460	37.8	0.5
203x203x9.5	6490	40.3	78.9	5964	75.6	1.0
102x102x6.4	2110	3.16	38.7	5855	151.3	2.0

TABLE 3 Total E_H ($/P_y\delta_y$)

Brace λ	Model	Loading protocol		
		AISC	ECCS	WC
0.5	Simple	52.77	57.19	54.03
	Refined	52.38	56.78	53.67
2.0	Simple	12.50	13.30	9.07
	Refined	12.43	13.23	9.04

TABLE 4 Test brace properties

No.	Shape	A (mm^2)	I ($10^6 mm^4$)	r (mm)	L (mm)	E (GPa)	F_y (MPa)	δ_y (mm)	v_o (mm)
S2A	102x76x4.8	1550	2.18	37.5	4614	185	381	7.79	4.6
S1QB	127x76x4.8	1790	3.78	45.9	4614	198	395	7.93	4.6
1B	127x127x8	3620	8.36	48.0	3401	191	421	8.30	3.0
2	152x152x8	4430	15.1	58.4	4900	190	467	10.5	3.0

TABLE 5 Test brace connection and slenderness properties

No.	C_g (kN-m/rad)	K ( )	KL (mm)	KL/r	λ	L_c (mm)	M_{pg} (kN-m)
S2A	63 (75)[(1)]	0.88	4051	108	1.56	19200 (16132)	3.68
S1QB	62 (75) [(1)]	0.93	4277	93.2	1.32	36210 (29940)	3.68
1B	1150	0.75	2545	52.6	0.79	4165	10.9
2	1290	0.76	3727	63.4	1.01	6672	12.1

[(1)]Value for the upper brace end, value in brackets for the lower brace end.

TABLE 6 Total E_H ($/P_y\delta_y$)

Case	Brace Specimen			
	S2A	S1QB	1B	2
Test	40.1	18.2	27.4	12.0
$n_e = 8$	40.5	14.5	23.4	8.57
$n_e = 16$	40.3	14.4	23.3	8.46
$n_e = 32$	40.2	14.4	23.3	8.45

Figure Captions

Fig. 1: Typical hysteretic response of steel bracing members (adapted from Tremblay et al., 2003).

Fig. 2: a) Fiber discretization; b) Typical hysteretic responses from computation.

Fig. 3: Influence of the element formulation, n_e and n_i on: a) Computational time; b) Mean quadratic error, *MQE*.

Fig. 4: Steel material models: a) Bi-linear model; b) Giuffré-Menegotto-Pinto model.

Fig. 5: Comparison of the predicted response obtained from the Giuffré-Menegotto-Pinto and bi-linear steel models for: a) $\lambda = 0.5$; b) $\lambda = 1.0$ ($n_e = 8$ and $n_f = 16$, $n_i = 3$).

Fig. 6: Influence of n_e and n_f on brace response parameters for: a) $\lambda = 2.0$; b) $\lambda = 1.0$; and c) $\lambda = 0.5$.

Fig. 7: Influence of test displacement protocol on brace energy dissipation: a) AISC displacement protocol; b) ECCS displacement protocol; and c) WC displacement protocol.

Fig. 8: Brace end connections: a) Typical brace connection; b) Plastic hinge in gusset plate upon brace buckling; c) Brace and gusset plate responses upon brace buckling; d) Brace model with length = *KL*; e) Brace model with extended brace segments; f) Brace model with zero-length end rotational springs.

Fig. 9: Comparison between test and pin-ended model with length *KL*: a) Hysteretic response with $R_0 = 25$, $a_1 = a_3 = 0.00001$, and $a_2 = a_4 = 0.00002$; b) Hysteretic response with $R_0 = 20$ and a_1 to $a_4 = 0.0$; c) Out-of-plane response at brace mid-length with $R_0 = 20$ and a1 to a4 = 0.0.

Fig. 10: Response of Specimen S2A using the brace model with end extensions: a) Comparison between test and predicted hysteretic responses; b) Comparison of the hysteretic responses predicted by the KL and the extension brace models; c) Comparison between test and predicted out-of-plane responses at brace mid-length.

Fig. 11: Validation of the response of Specimen S2A from the model with rotational end springs (n_f = 6, n_i = 3, n_e = 8): a) Upper gusset plate moment-rotation hysteresis;b) Comparison of test and predicted upper gusset plate rotation; c) Comparison of test and predicted brace hysteretic axial response; and d) Comparison of test and predicted brace out-of-plane response.

Fig. 12: Comparison between test and predicted brace hysteretic axial and out-of-plane responses for: a) Specimen S1QB; b) Specimen 1B; and c) Specimen 2.

Fig. 13: Full scale frame test: a) Test Setup for Specimen X6-C (adapted from Tremblay et al., 2003); b) Frame model.

Fig. 14: Response of test frame X6-C: a) Comparison between test and predicted (n_e = 4) lateral load-lateral deformation hysteretic responses; b) Out-of-plane deformation response at the lower half-brace segment; c) Out-of-plane deformation response at the brace intersection point; d) Influence of n_e on the lateral load-lateral deformation response prediction; and e) Influence of n_e on the energy dissipation prediction.

Fig. 15: Seismic response of a single-storey X-braced steel frame building: a) Time history of roof displacement and dissipated energy; b) Influence of time step on base shear-roof displacement hysteretic response.

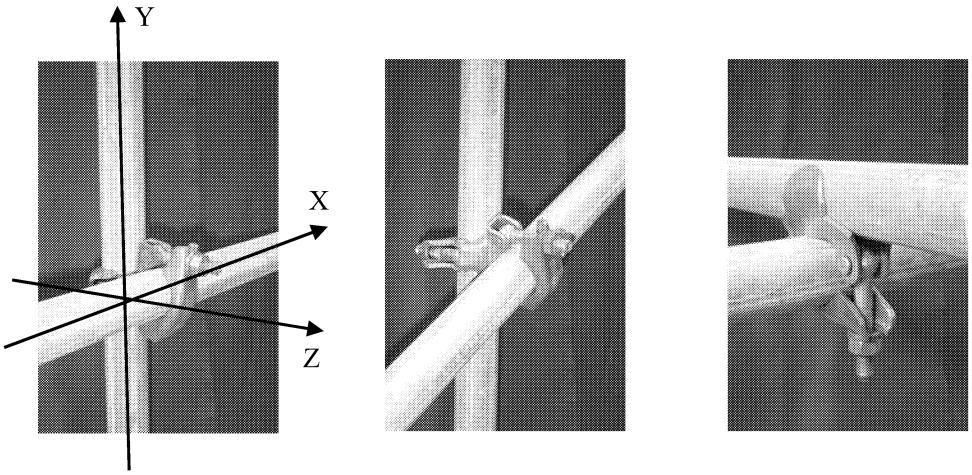

(a) right-angle coupler (b) Swivel coupler (c) Putlog coupler

Figure 1. Three types of scaffolding coupler

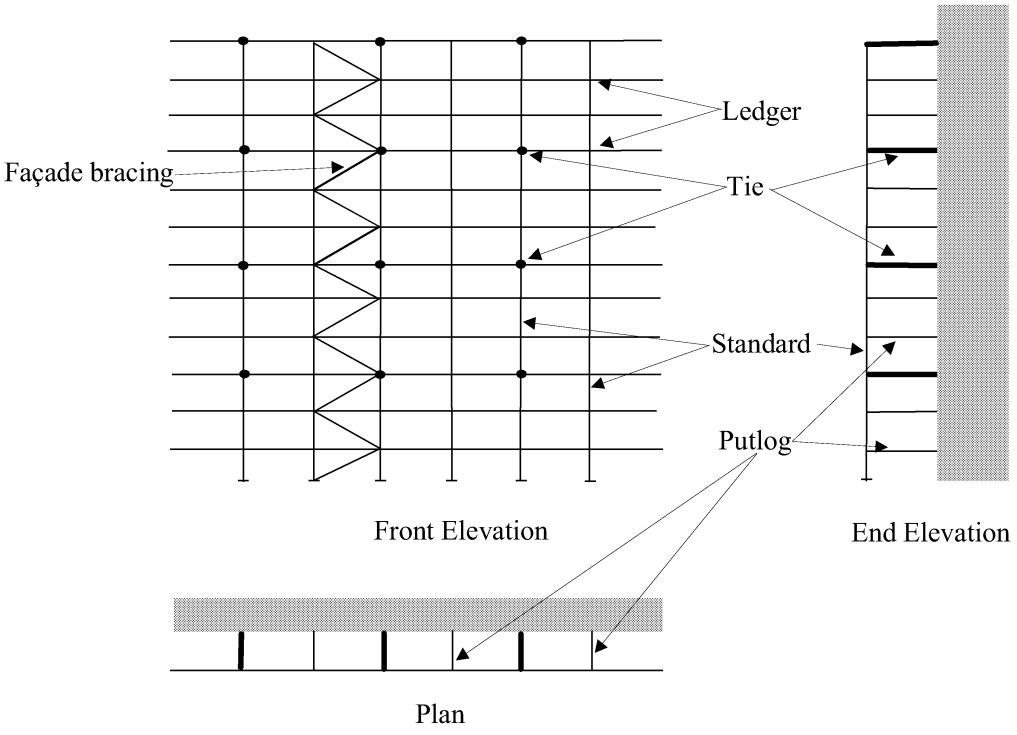

Figure 2. Typical Putlog Scaffold

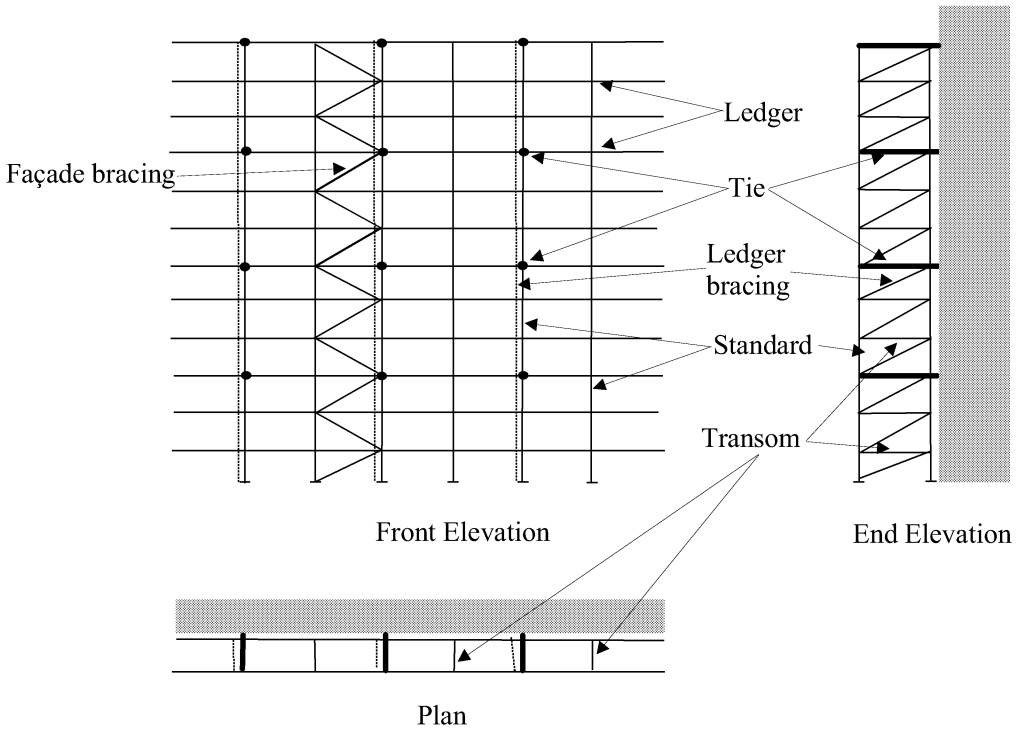

Figure 3. Typical Independent Tied Scaffold

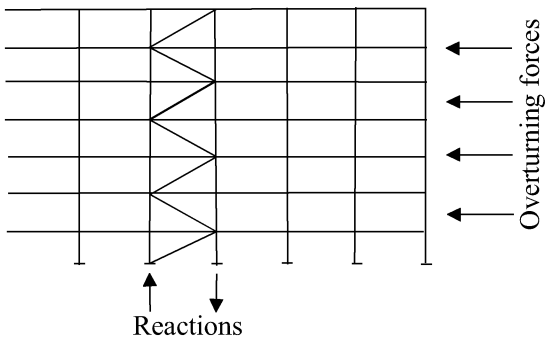

Figure 4. Bracing action under side loads

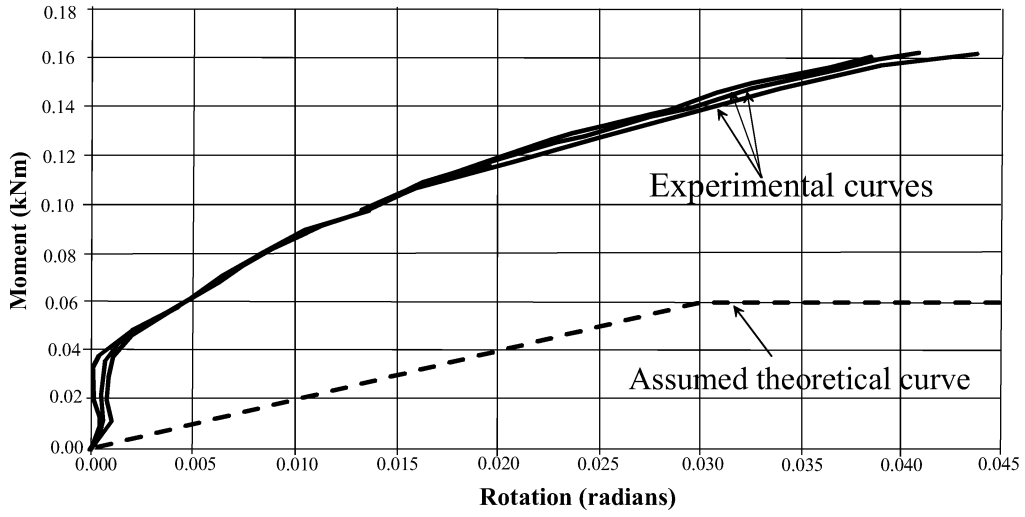

Figure 5. Moment-Rotation Characteristics for a Putlog Coupler

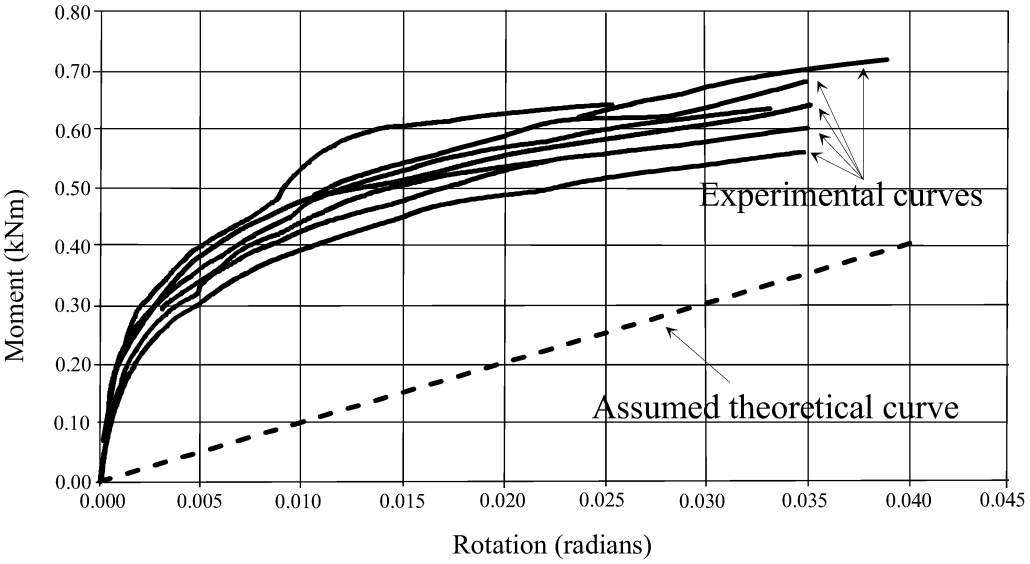

Figure 6. Moment–Rotation Characteristics for a Right Angle Coupler

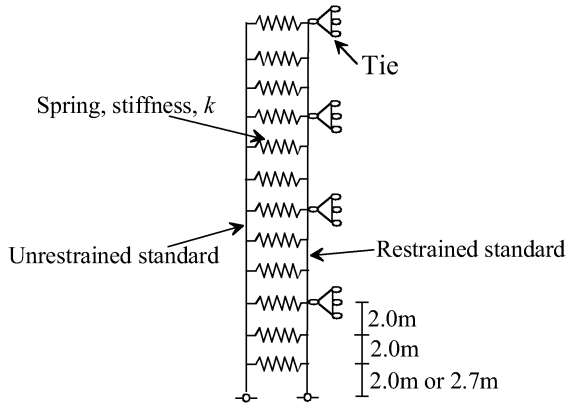

Figure 7. Two column Putlog model for buckling normal to the facade

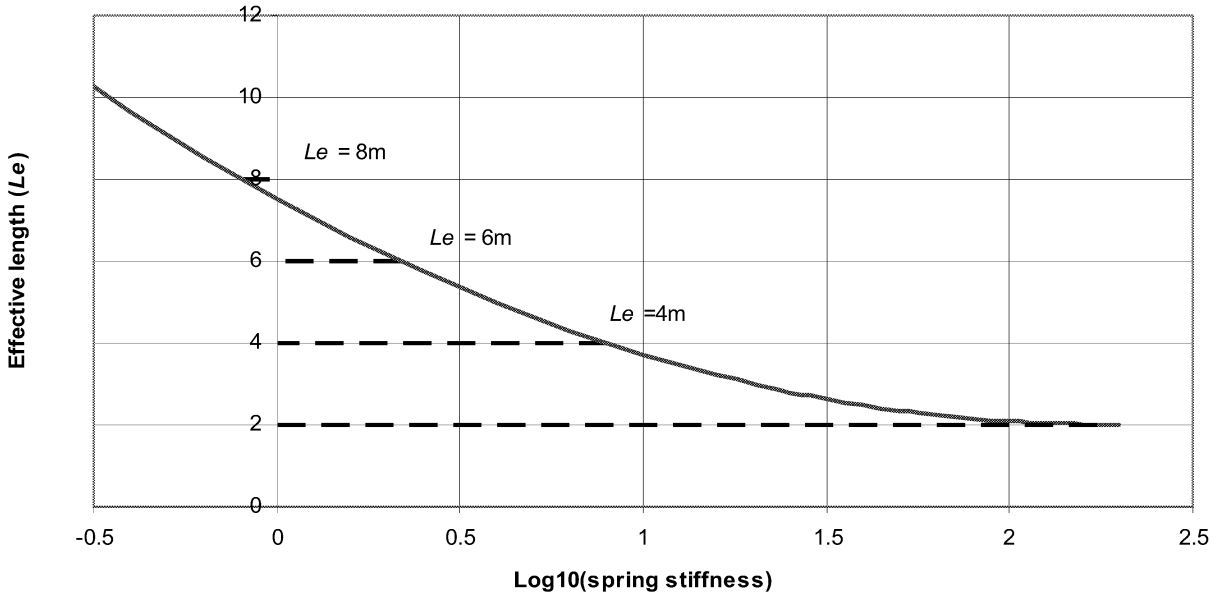

Figure 8. Variation of effective length with spring stiffness

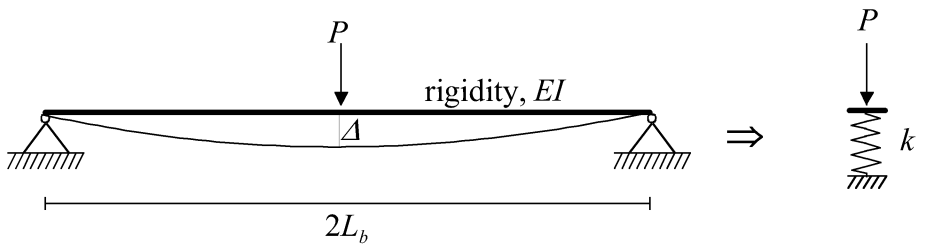

Figure 9. Derivation of stiffness for 'pinned' ledgers

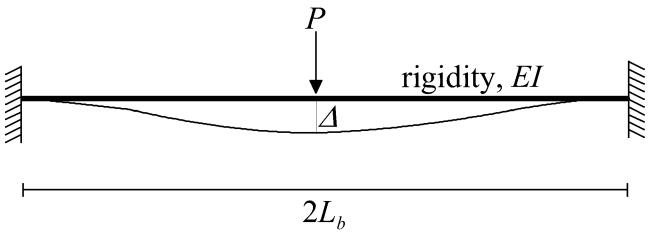

Figure 10. Derivation of stiffness for 'fixed' ledgers

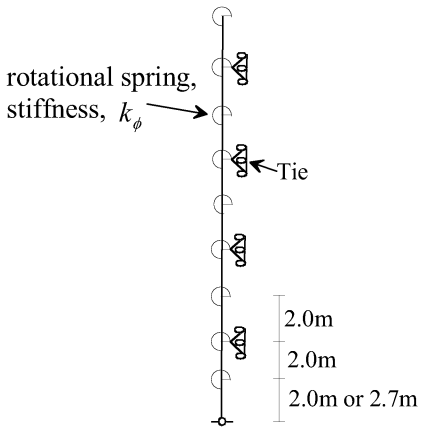

Figure 11. Single column model for the rear face of a tied scaffold

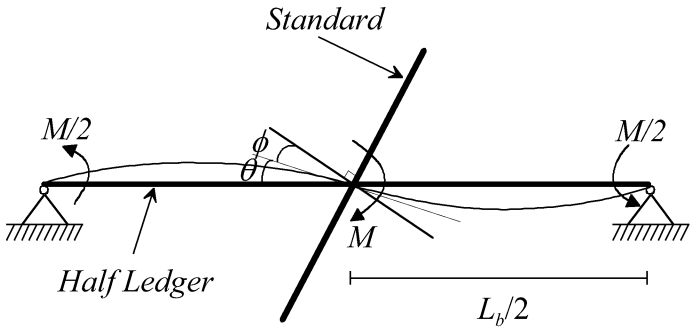

Figure 12. Derivation of rotation stiffness for standard-ledger connection in double curvature

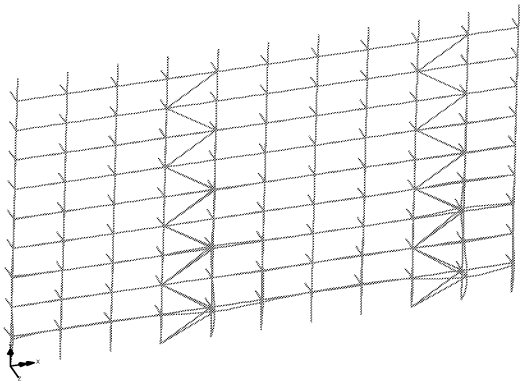

(a) Buckling of leeward braced standard normal to the facade for a Putlog scaffold

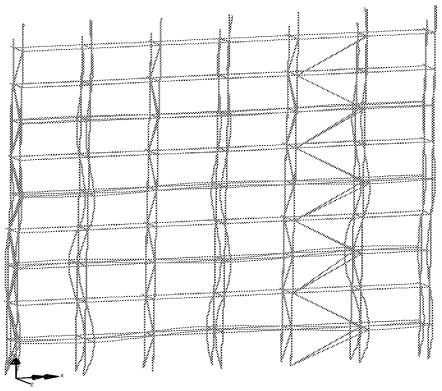

(b) Buckling of independent tied scaffold normal to the façade

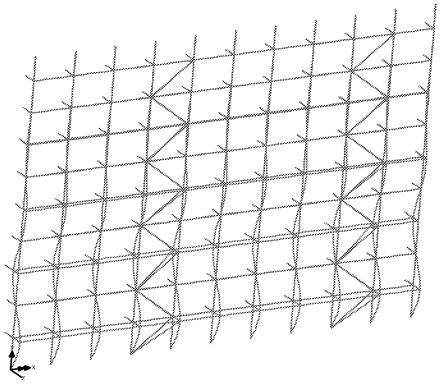

(c) Uniform buckling of Putlog scaffold normal to the facade

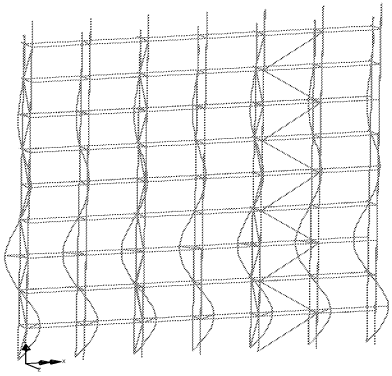

(d) Buckling of tied scaffold parallel to the facade (only the rear face buckles)

Figure 13. Examples of buckling modes

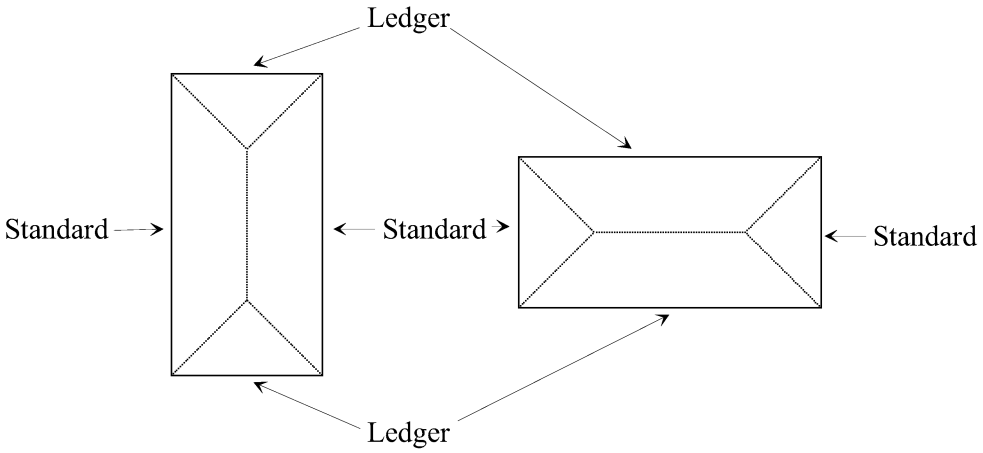

Figure 14. Wind load distribution patterns

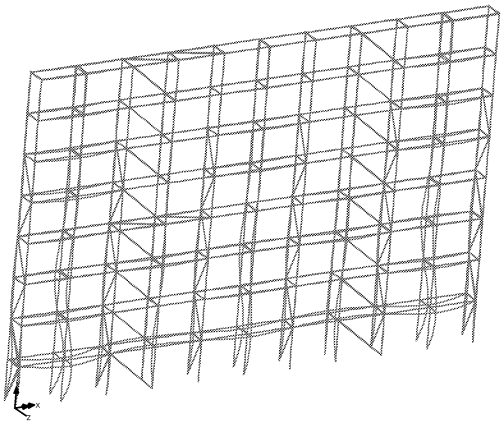

(a) tied scaffold buckling normal to facade

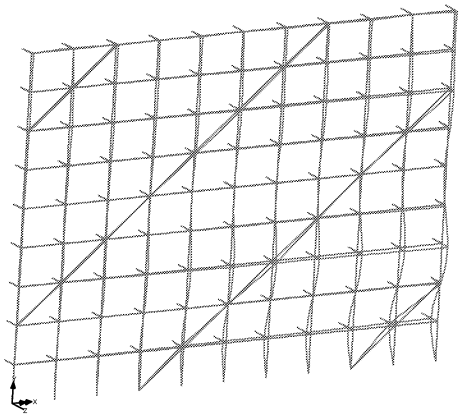

(b) Putlog scaffold buckling normal to facade

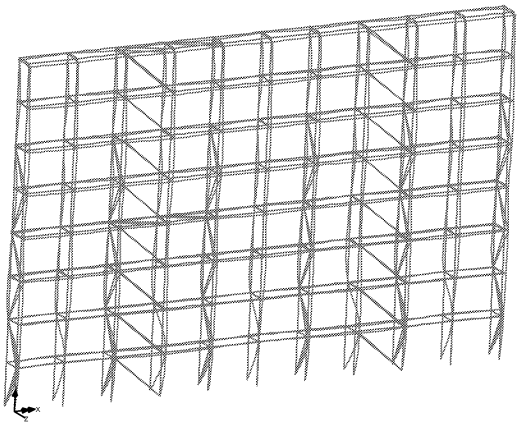

(c) tied scaffold with rear face buckling parallel to facade

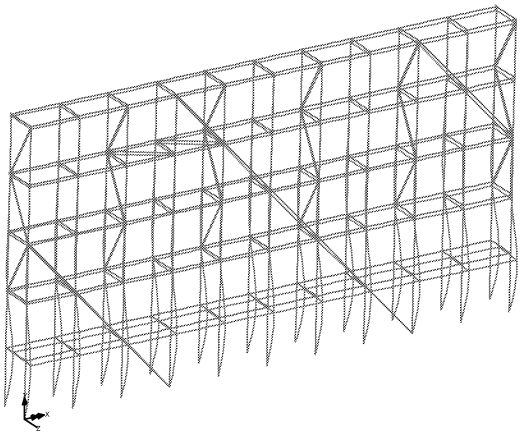

(d) tied scaffold buckling normal to facade with no ledger bracing in bottom two lifts

Figure 15. Examples of ultimate failure modes

Table 1. Effective lengths for Putlog scaffolds found from the two-dimensional model

	Tie Interval	Span = 2.7m	Span = 2.1m	Span = 1.8m
Simply Supported Ledgers	2m	3.94	3.17	2.77
	4m	4.06	4.00	4.00
	6m	6.00	6.00	6.00
	8m	8.00	8.00	8.00
Fixed Ended Ledgers	2m	2.64	2.18	2.02
	4m	4.00	4.00	4.00
	6m	6.00	6.00	6.00
	8m	8.00	8.00	8.00

Table 2. Tie Patterns

Case	Tie position above base (m)								
1	2.7	4.7	6.7	8.7	10.7	12.7	14.7	16.7	18.7
2	2.7		6.7		10.7		14.7		18.7
3	2.7			8.7			14.7		18.7
4	2.7				10.7				18.7
5	2.0	4.0	6.0	8.0	10.0	12.0	14.0	16.0	18.0
6		4.0		8.0		12.0		16.0	18.0
7			6.0			12.0			18.0
8				8.0				16.0	18.0
9	2.0		6.0		10.0		14.0		18.0
10	2.0			8.0			14.0		18.0
11	2.0				10.0				18.0

Table 3. Effective lengths of Putlog scaffolds for different bay widths
buckling normal to the façade determined by the three-dimensional analysis

Case	1.8m	2.1m	2.7m
1	2.83	3.17	3.94
2	3.91	3.92	3.99
3	5.03	5.04	5.06
4	7.24	7.24	7.26
5	2.77	3.16	3.94
6	3.90	3.91	4.03
7	6.00	6.00	6.00
8	7.20	7.21	7.25
9	3.90	3.91	3.99
10	4.99	4.99	5.02
11	7.39	7.20	7.35

Table 4. Effective lengths of independent tied scaffold with full ledger bracing

	Parallel to façade			Normal to facade		
Case	1.8m	2.1m	2.7m	1.8m	2.1m	2.7m
1	2.39	2.29	2.29	2.83	3.17	3.94
2	3.42	3.42	3.43	2.85	3.19	3.95
3	4.16	4.16	4.18	2.87	3.21	3.95
4	5.03	5.04	5.01	2.90	3.27	4.01
5	1.90	1.90	1.90	2.77	3.16	3.94
6	3.56	3.56	3.56	2.78	3.18	3.95
7	4.81	4.81	4.83	2.90	3.25	3.98
8	5.55	5.57	5.57	3.29	3.18	3.96
9	3.40	3.41	3.41	2.84	3.19	3.95
10	4.12	4.13	4.13	2.86	3.21	3.95
11	5.00	5.02	5.04	2.90	3.26	4.01

Table 5. Effective lengths of independent tied scaffold with partial ledger bracing

		Parallel			Normal		
Description	Case	1.8m	2.1m	2.7m	1.8m	2.1m	2.7m
No bottom brace	2	3.46	3.47	3.47	3.21	3.37	3.57
	9	3.45	3.45	3.45	3.20	3.36	3.56
No brace in bottom two	2	3.46	3.47	3.47	3.21	3.38	3.57
levels	9	3.45	3.45	3.45	3.20	3.36	3.56
No brace in second and third	2	3.42	3.42	3.42	3.26	3.40	3.58
levels from bottom	9	3.40	3.41	3.41	3.22	3.37	3.56
No ledger brace	2	3.41	3.42	3.43	3.70	3.74	3.81
	6	3.56	3.56	3.56	3.75	3.77	3.81
	9	3.40	3.40	3.41	3.69	3.73	3.81

Table 6. Weights of scaffold components

Component	Weight
Coupler	1.8 kg
Ledger, standard, putlog, guard-rail	4.37 kg/m
Toe board	5.36 kg/m

Table 7. Table of loads

Class	Load intensity (kN/m²)	Reduction factor	No. of Boards	Bay width (m)
1	0.75	0.00	3	2.7
2	1.50	0.25	4	2.4
3	2.00	0.25	5	2.1
4	3.00	0.50	5	1.8

Table 8. Scaffolds Analysed

Scaffold type	Ref. No.	Class	Sheeted or not	Boarded or not	Ledger bracing	Wind Storm param. **S**	T or C	Dist. to Sea	No of levels	Facade bracing
Putlog	1	1	not	yes	N/A	20	T	100	6	2 bays in 5
Putlog	2	2	not	not	N/A	24	C	0.1	9	5 bays in 5
Independent	3	2	not	yes	part	20	T	10	8	1 bay in 5
Independent	4	3	debris	not	full	24	C	10	17	2 bays in 5
Independent	5	4	sheeted	yes	part	28	T	0.1	5	5 bays in 5
Putlog	6	1	not	not	N/A	28	T	10	6	2 bays in 5
Independent	7	3 cant	not	yes	part	40	T	0.1	8	1 bay in 5
Independent	8	4 cant	not	not	full	40	C	100	17	5 bays in 5
Independent	9	1	debris	yes	full	32	T	0.1	8	2 bays in 5
Independent	10	4	sheeted	not	part	32	T	100	5	5 bays in 5

Table 9. Results of analyses

Ref. No.	Load case giving maximum limit state	Max k at T_λ =1	Max T_λ	Mode
1	Service wind, normal to facade	0.696	6.360	Buckling normal to facade
2	Service wind, normal to facade	0.375	2.130	Buckling normal to facade
3	Service wind, normal to facade	0.730	1.845	Buckling normal to facade
4	Service wind, parallel to façade	0.458	1.947	Buckling parallel to facade
5	Out-of-service wind, parallel to facade	1.006	2.641	Buckling normal to facade
6	Out-of-service wind, normal to façade	0.549	3.000	Not buckled, maximum increments exceeded
7	Out-of-service wind, parallel to facade	0.984	1.575	Not buckled, convergence failure
8	Out-of-service wind, parallel to façade	1.072	2.407	Not buckled, excessive bending in ledger
9	Out-of-service wind, parallel to facade	0.975	3.000	Not buckled, maximum increments exceeded
10	Out-of-service wind, parallel to facade	0.730	3.000	Not buckled, maximum increments exceeded

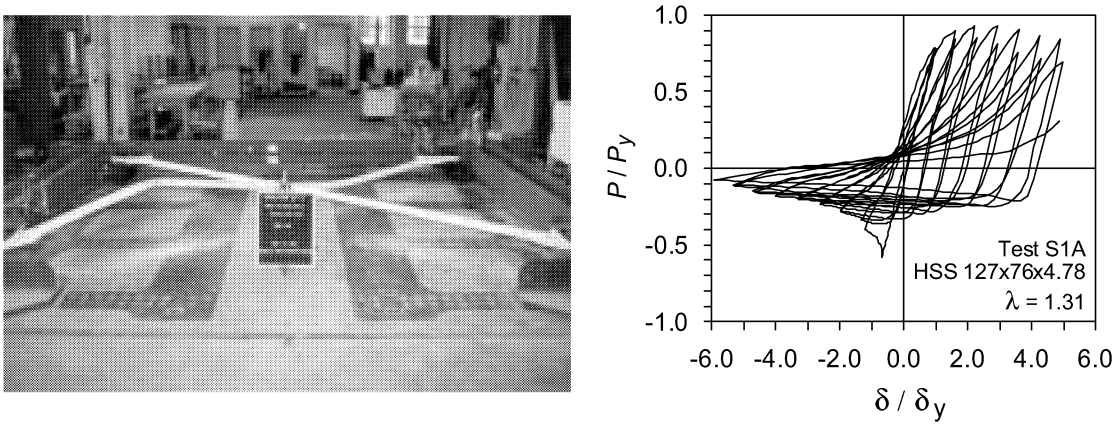

Fig. 1 Agüero et al.

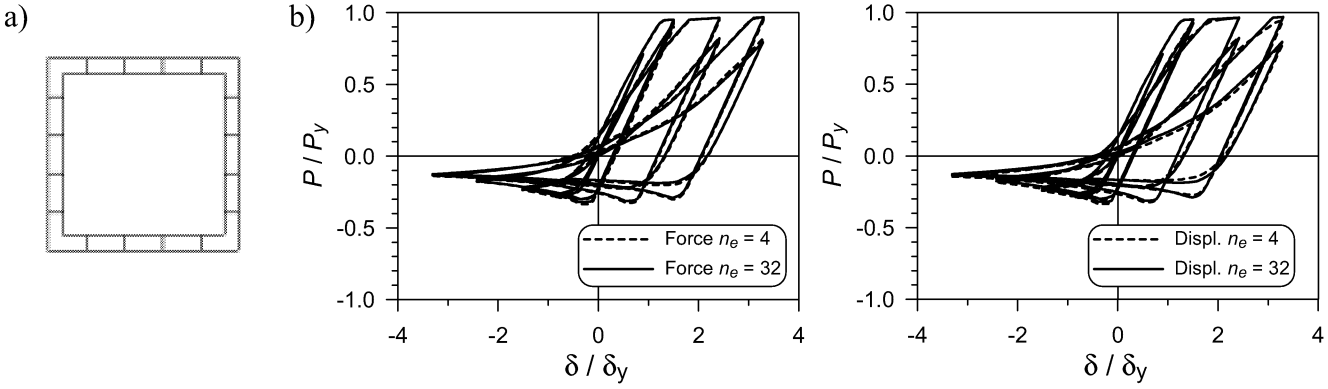

Fig. 2 Agüero et al.

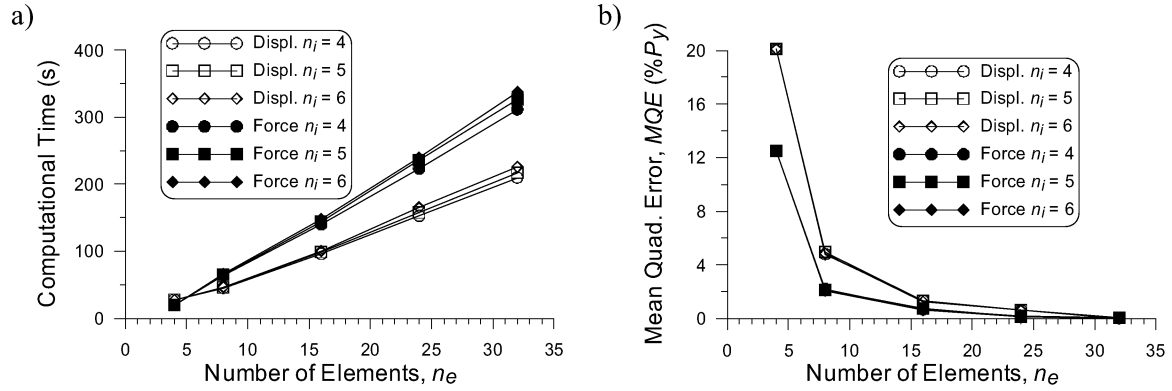

Fig. 3 Agüero et al.

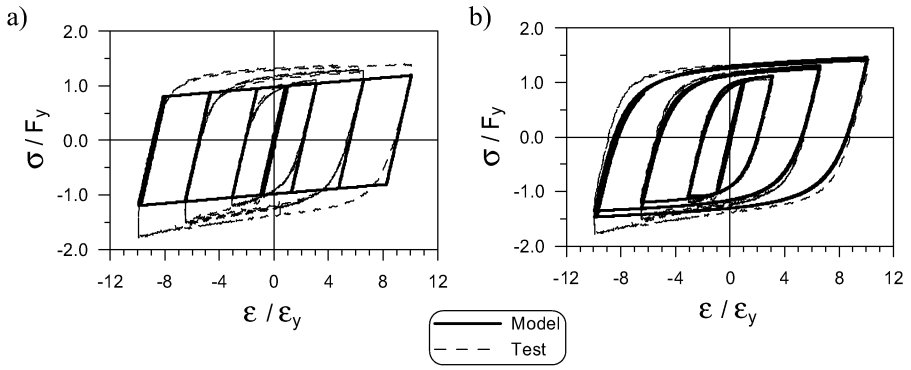

Fig. 4 Agüero et al.

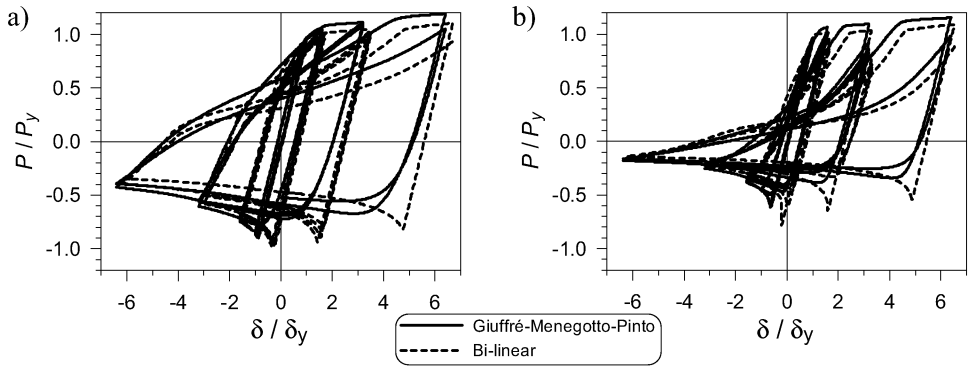

Fig. 5 Agüero et al.

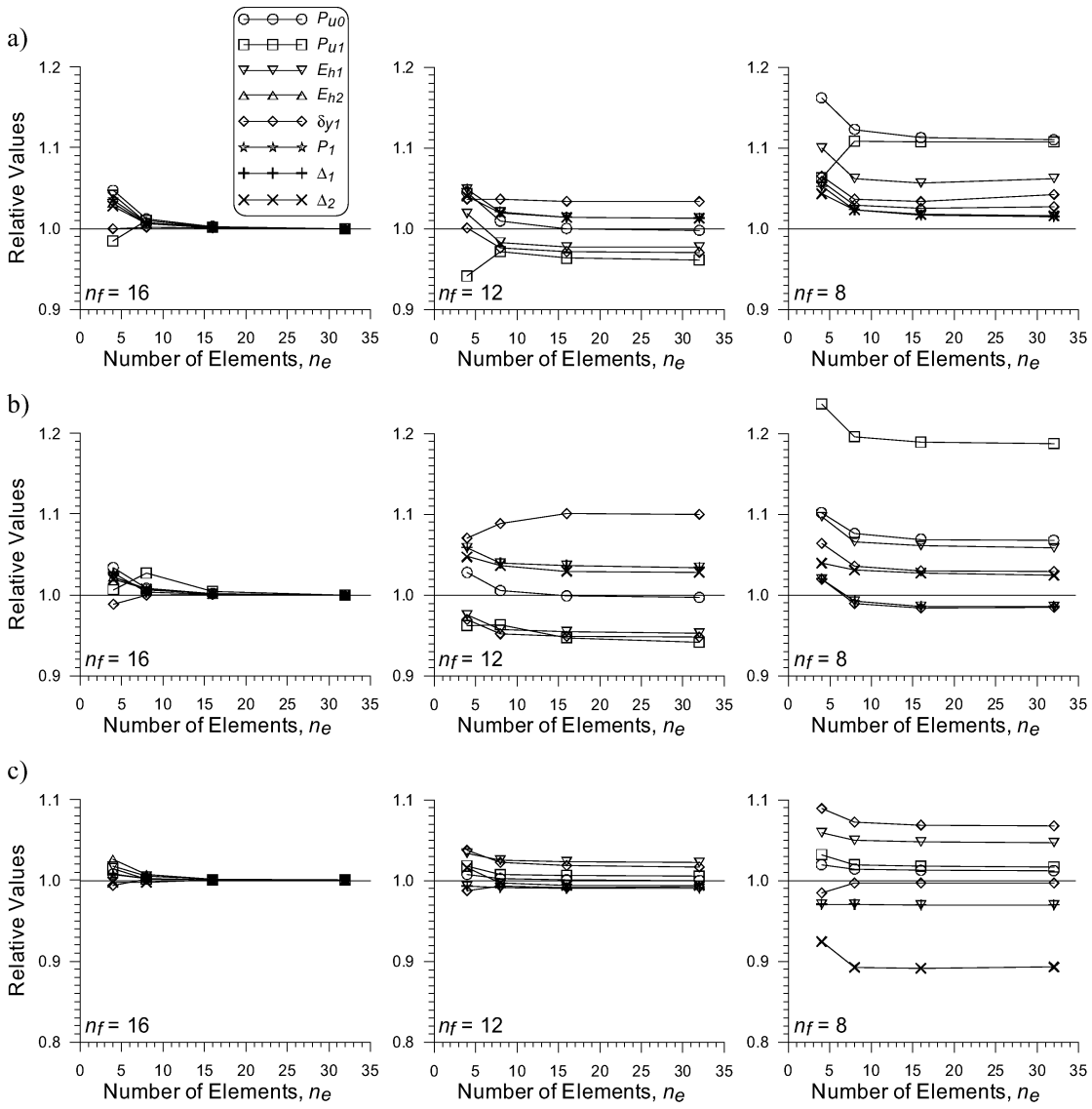

Fig. 6 Agüero et al.

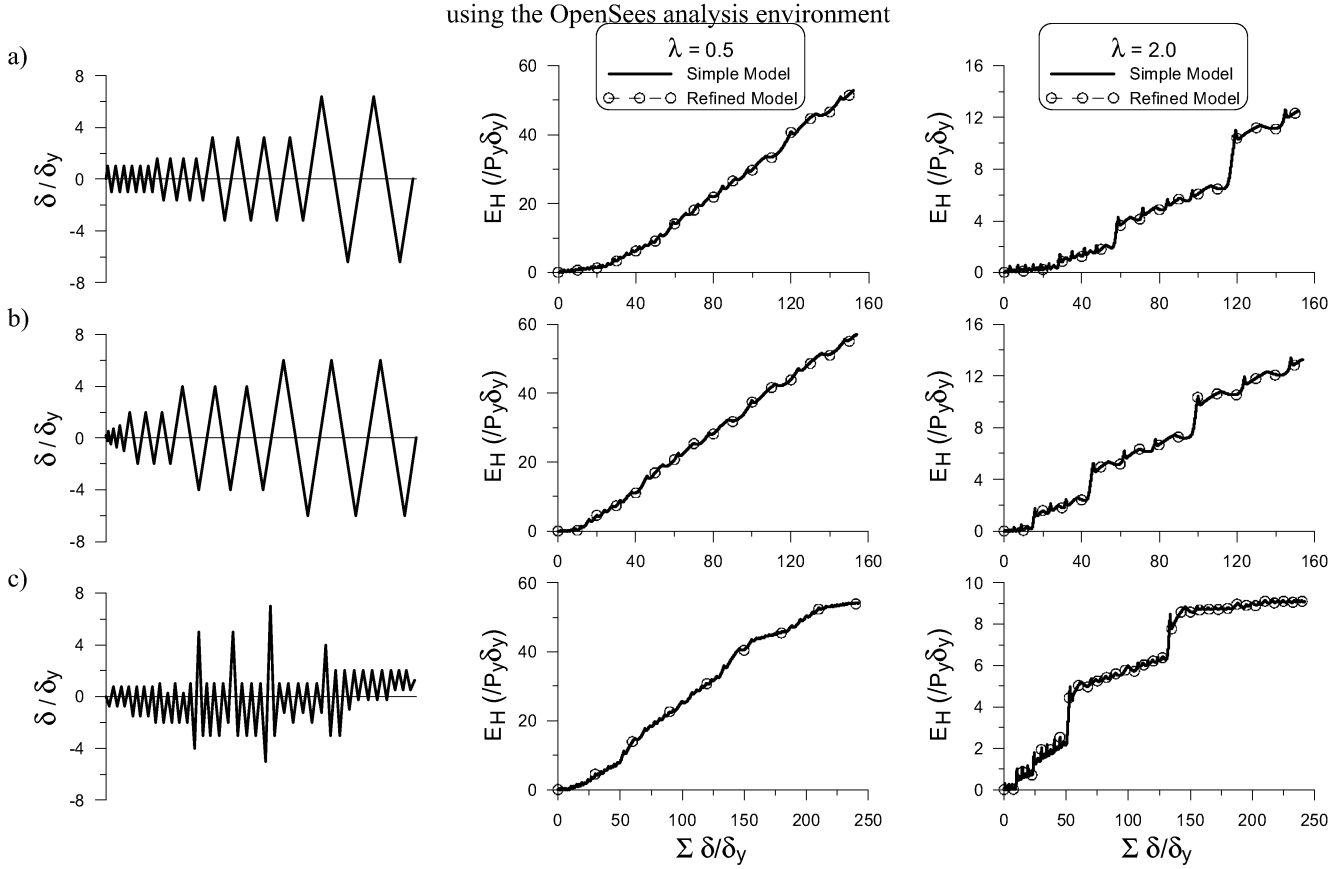

Fig. 7 Agüero et al.

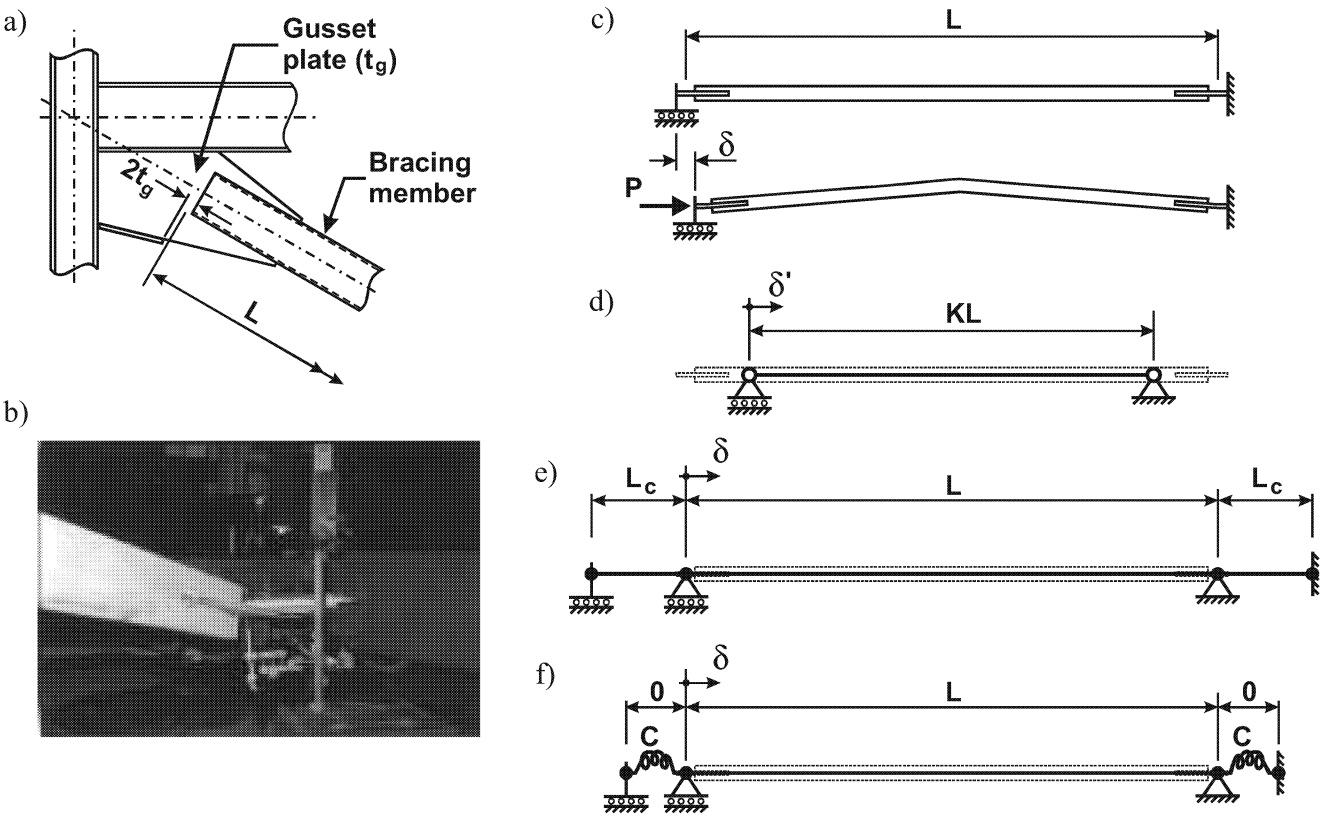

Fig. 8 Agüero et al.

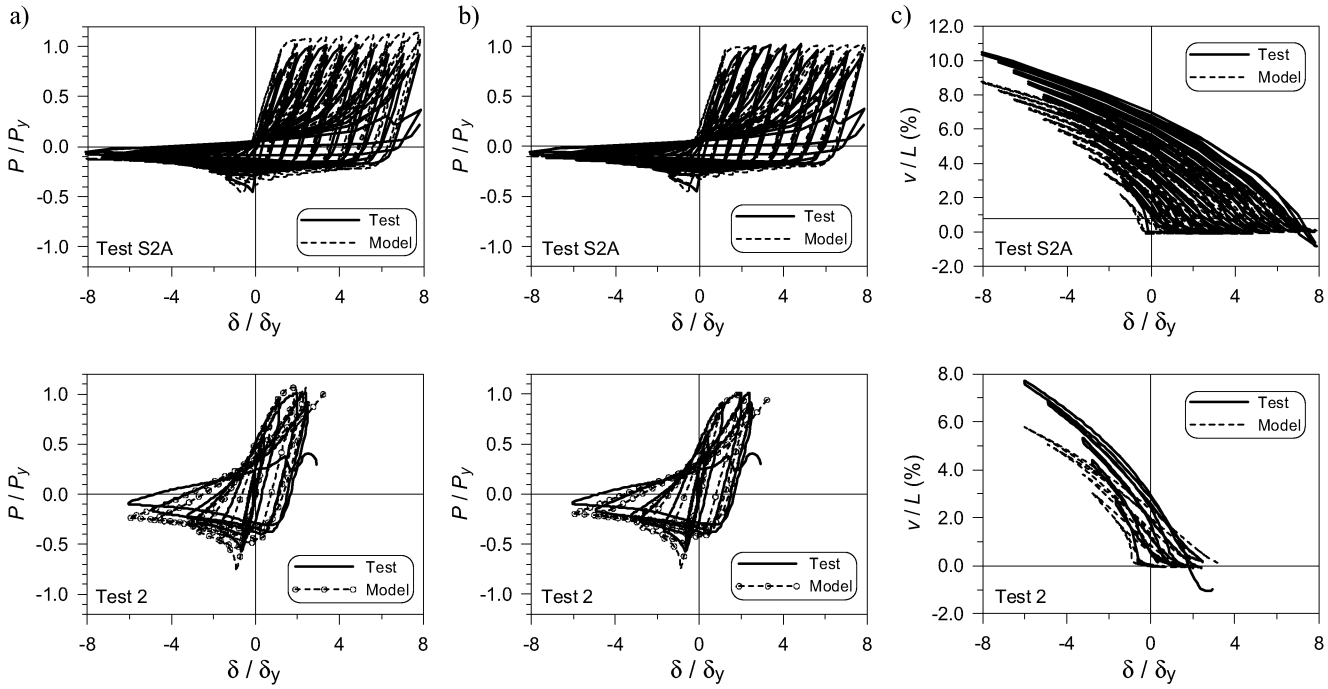

Fig. 9 Agüero et al.

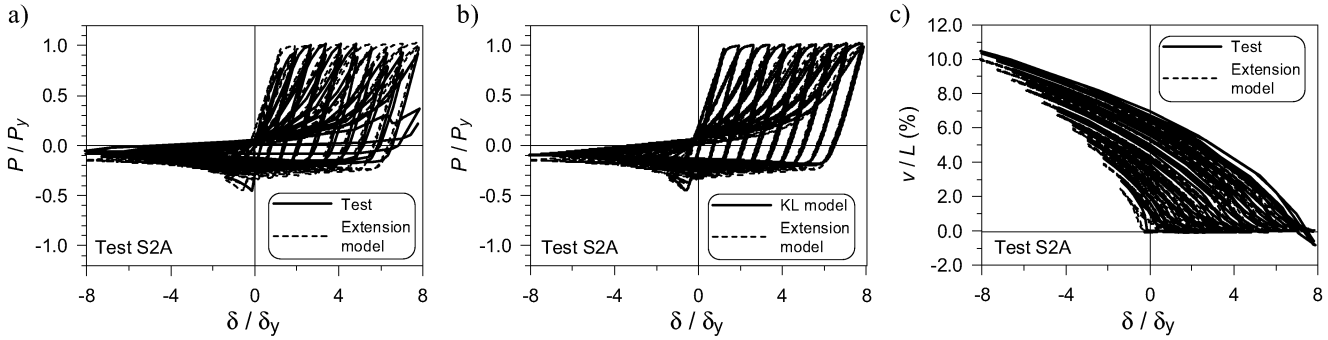

Fig. 10 Agüero et al.

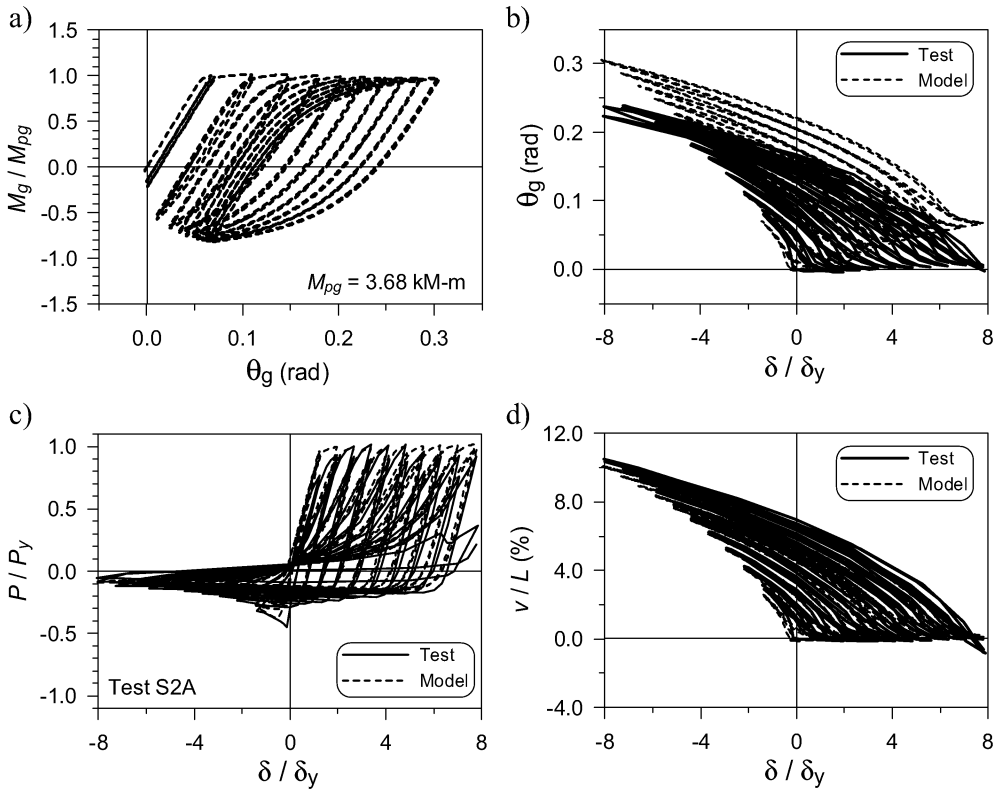

Fig. 11 Agüero et al.

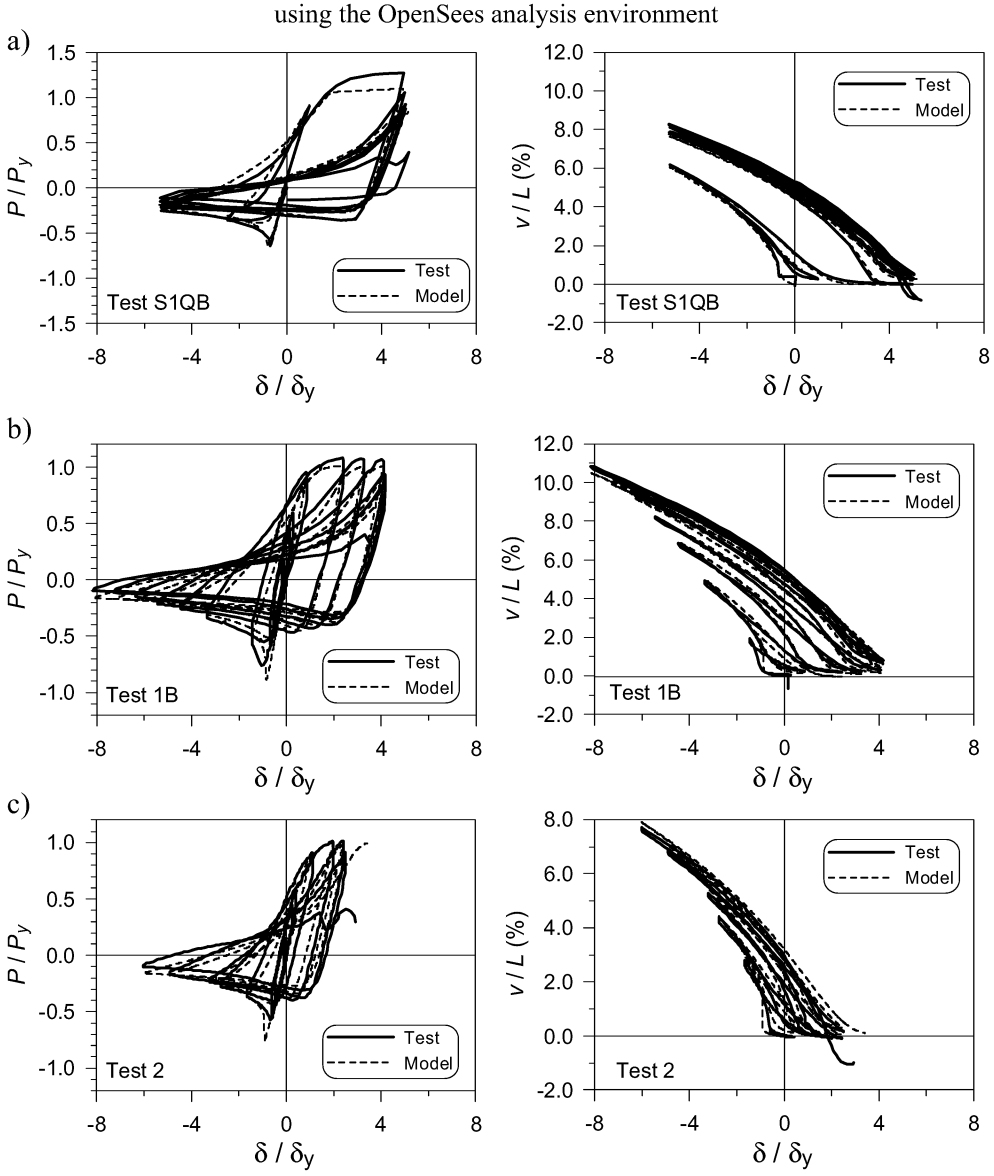

Fig. 12 Agüero et al.

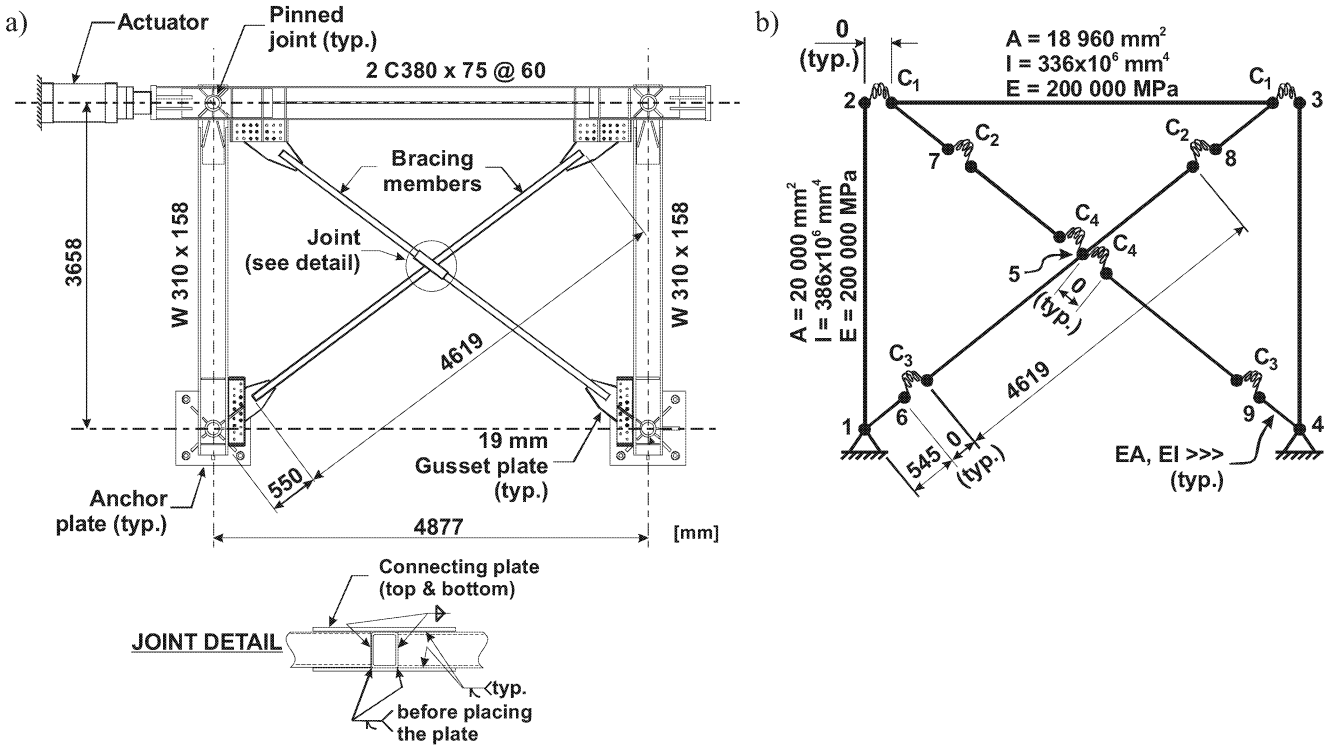

Fig. 13 Agüero et al.

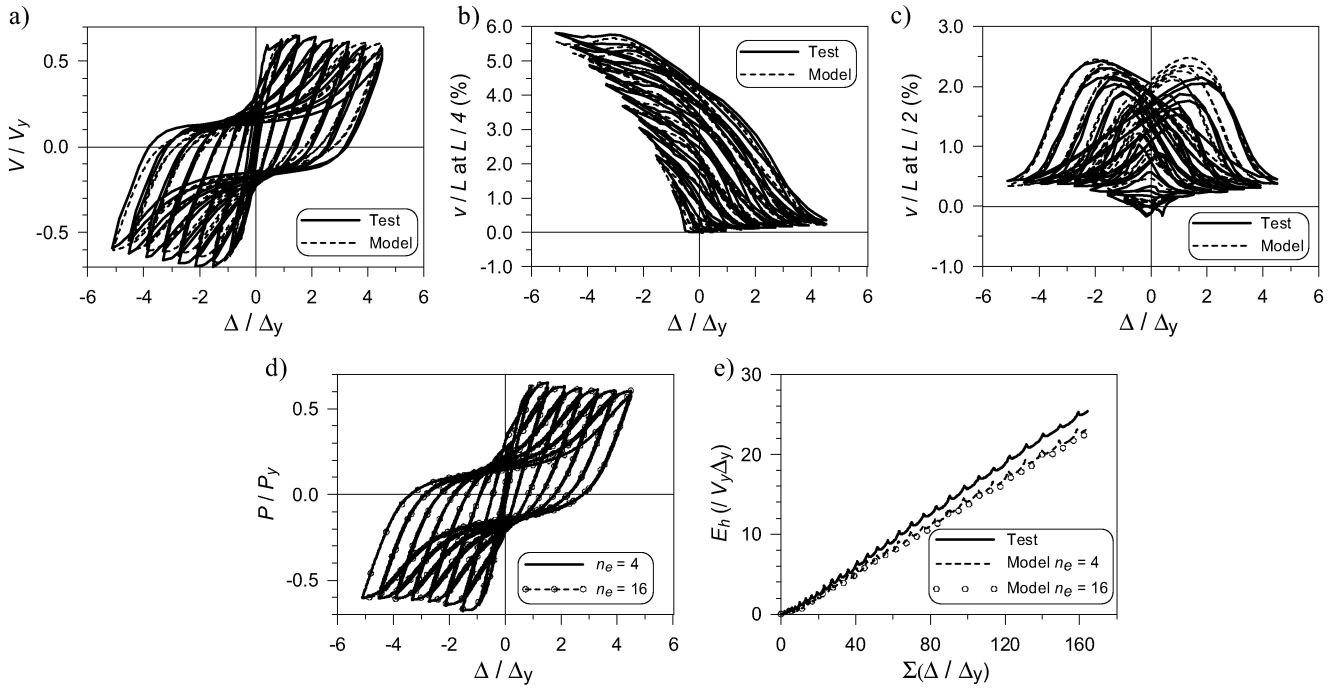

Fig. 14 Agüero et al.

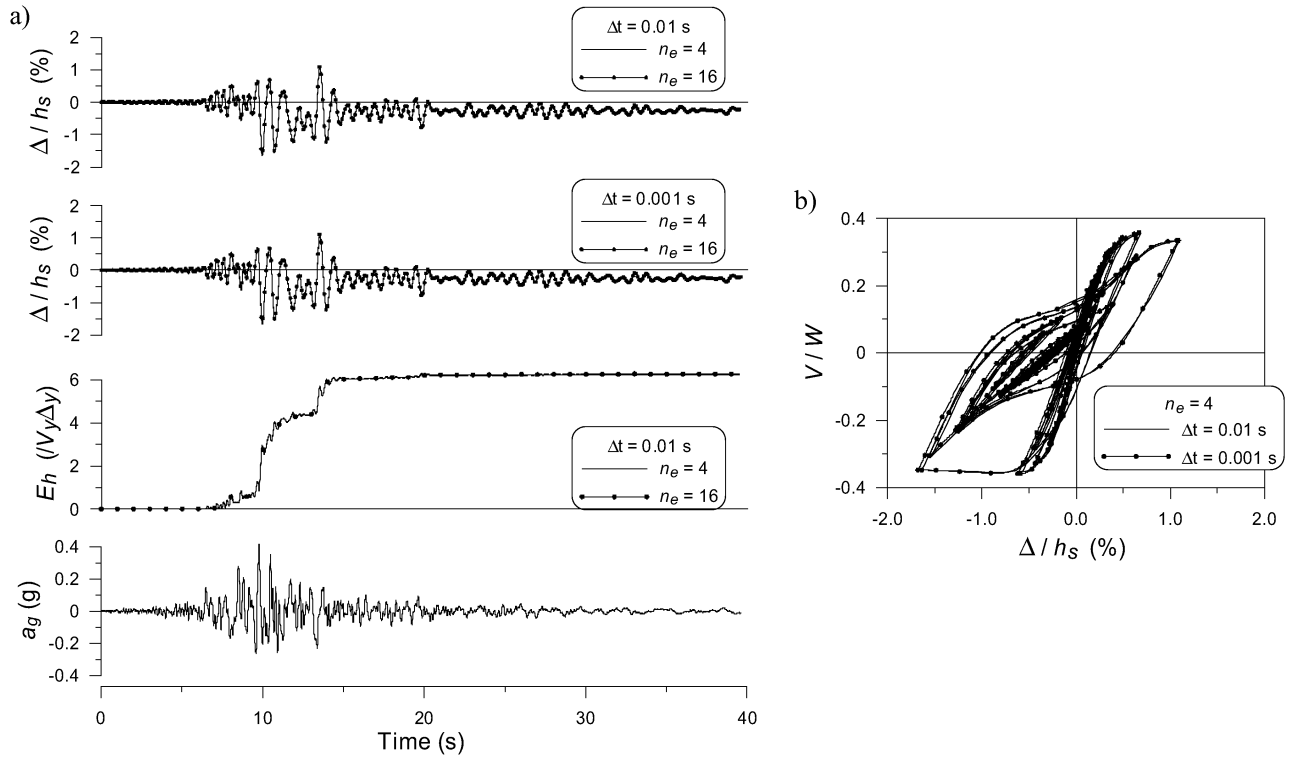

Fig. 15 Agüero et al.